



Flow and entrapment of dense nonaqueous phase liquids in physically and chemically heterogeneous aquifer formations

Scott A. Bradford*, Linda M. Abriola & Klaus M. Rathfelder

University of Michigan, Department of Civil and Environmental Engineering, 181 EWRE, 1351 Beal Avenue, Ann Arbor, MI 48109-2125, USA

(Received 17 September 1997; accepted 3 March 1998)

The migration and entrapment of dense nonaqueous phase liquids (DNAPLs) in aquifer formations is typically believed to be controlled by physical heterogeneities. This belief is based upon the assumption that permeability and capillary properties are determined by the soil texture. Capillarity and relative permeability, however, will also depend on porous medium wettability characteristics. This wettability may vary spatially in a formation due to variations in aqueous phase chemistry, contaminant aging, and/or variations in mineralogy and organic matter distributions. In this work, a two-dimensional multiphase flow simulator is modified to simulate coupled physical and chemical formation heterogeneity. To model physical heterogeneity, a spatially correlated permeability field is generated, and then related to the capillary pressure-saturation function according to Leverett scaling. Spatial variability of porous medium wettability is assumed to be correlated with the natural logarithm of the intrinsic permeability. The influence of wettability on the hysteretic hydraulic property relations is also modeled. The simulator is then employed to investigate the potential influence of coupled physical and chemical heterogeneity on DNAPL flow and entrapment. For reasonable ranges of wettability characteristics, simulations demonstrate that spatial variations in wettability can have a dramatic impact on DNAPL distributions. Higher organic saturations, increased lateral spreading, and decreased depth of infiltration were predicted when the contact angle was varied spatially. When chemical heterogeneity was defined by spatial variation of organic-wet solid fractions (fractional wettability porous media), however, the resultant organic saturation distributions were more similar to those for perfectly water-wet media, due to saturation dependent wettability effects on the hydraulic property relations. © 1998 Elsevier Science Limited. All rights reserved

Keywords: multiphase flow, NAPL, wettability, heterogeneity, numerical model.

NOMENCLATURE

D	denotes drainage	I	denotes imbibition
f	weighting function	k	intrinsic permeability (m^2)
F_o	organic wet mass fraction	k_{avg}	average intrinsic permeability (m^2)
g	acceleration due to gravity (m/s^2)	k_{ro}	relative permeability of organic
		k_{rw}	relative permeability of water
		m	parameter equal to $1 - 2/n$

*Corresponding author. Tel: +1 313 936-3175; fax: +1 313 763-2275; e-mail: sbrad@engin.umich.edu

n	pore size distribution parameter of van Genuchten ⁷² capillary pressure model	S_{wmin}	minimum wetting fluid saturation (cm^3/cm^3)
o	organic liquid	\bar{S}^{eff}	effective saturation
P_c	capillary pressure (N/m^2 , cm water)	\bar{S}^{app}	apparent saturation
P_c^{ref}	capillary pressure at reference location (N/m^2 , cm water)	w	water
P_c^*	capillary pressure that accounts for wettability (N/m^2 , cm water)	\mathbf{x}	two-dimensional spatial coordinate vector (m,m)
P_o	pressure of organic phase (N/m^2 , cm water)	z	vertical direction (m)
P_w	pressure of water phase (N/m^2 , cm water)	α	parameter for reciprocal of entry pressure ($1/\text{cm}$)
Q	source/sink term ($\text{g}/\text{cm}^3\text{s}$)	β	correlation coefficient
R	pore radius (cm)	ε	porosity (cm^3/cm^3)
s	solid	λ^{ref}	shifting parameter at reference location (cm)
S	saturation (cm^3/cm^3)	λ_{hys}^{ref}	hysteretic shifting parameter at reference location (cm)
S_{io}	'immobile' organic saturation (cm^3/cm^3)	μ	viscosity of the fluid (g/cms)
S_{iw}	'immobile' water saturation (cm^3/cm^3)	ξ	chemical heterogeneity (F_o or ϕ_{sow})
S_{ot}	entrapped organic saturation (cm^3/cm^3)	ξ_{avg}	average chemical heterogeneity (F_o or ϕ_{sow})
S_{omax}	maximum organic saturation (cm^3/cm^3)	ξ_n	normalizing factor for chemical heterogeneity (180° or 1)
S_{omin}	minimum organic saturation (cm^3/cm^3)	ρ	density of the fluid (g/cm^3)
S_{mot}	maximum entrapped organic saturation (cm^3/cm^3)	σ_{ow}	interfacial tension (N/m)
S_{mwt}	maximum entrapped water saturation (cm^3/cm^3)	ϕ_{sow}	equilibrium contact angle (degree)
S_{ro}	residual organic saturation (cm^3/cm^3)		
S_{ro}^*	residual organic saturation that accounts for wettability (cm^3/cm^3)		
S_{rw}	residual water saturation (cm^3/cm^3)		
S_{rw}^*	residual water saturation that accounts for wettability (cm^3/cm^3)		
S_{wt}	entrapped water saturation (cm^3/cm^3)		
S_{wmax}	maximum water saturation (cm^3/cm^3)		
S_{wmin}	minimum water saturation (cm^3/cm^3)		

1 INTRODUCTION

The flow and entrapment of nonaqueous phase liquids (NAPLs) in the saturated zone is typically believed to be controlled by layers and lenses of contrasting soil texture.^{20,32,45,60,73} Inherent in previous studies is the assumption that water preferentially wets the soil surfaces. Under such conditions, water will be retained by capillary forces in smaller pores and/or finer textured soil, whereas the NAPL will be found in larger pores and/or coarser textured material. In multiphase scenarios, the ability of the soil to transmit water and NAPL will be governed by the spatial and temporal saturation distribution, as well as by the aquifer intrinsic permeability structure. Physical heterogeneity also affects NAPL entrapment, which may occur due to

pore-scale processes such as snap-off,¹⁸ or larger scale processes such as aqueous phase by-passing of NAPL filled coarse texture layers,⁷³ and NAPL pooling above low permeability layers. With their focus on soil texture variations, the aforementioned studies have failed to consider the potential influence of chemical heterogeneities, i.e. spatially varying wettability, on NAPL transport and capillary retention.

Wettability, the pore-scale distribution of immiscible fluids near solid surfaces, significantly influences the capillary pressure⁶ and relative permeability²⁷ relations. Furthermore, residual NAPL saturation is known to be sensitive to medium wettability.⁵⁶ In natural porous media the wettability can vary spatially due to contaminant aging,⁶² and/or variations in aqueous chemistry,²³ mineralogy,⁴ organic matter distributions,²¹ and surface roughness.⁵⁴ Wettability effects on hydraulic property relations have been reported to be saturation independent^{25,55} or saturation dependent.^{12,13,15,28,66} The latter can occur in fractional wettability porous media due to the presence of water (w) and organic (o) wet solids. In the petroleum literature, fractional wettability has been recognized as a ubiquitous condition.⁴⁻⁷

The manipulation of soil wettability has been proposed for use in remediation or contaminant migration control through the emplacement of organic-wet zones or the creation of *in situ* chemical reactions.^{17,35,36,75} For example, Hayworth and Burris³⁵ proposed the use of cationic surfactants to create an enhanced sorption zone for miscible organic contaminants. Remediation options such as the use of nonionic surfactants or biodegradation could subsequently be employed within this enhanced sorbent zone to remove the retained organic contaminants from the aquifer. Note that such remediation approaches are not limited to sorption of soluble organic contaminants, these methods could equally be applied to separate phase organic liquids which are retained by capillary forces in organic-wet zones. The use of organic-wet capillary barriers near landfills and/or underground storage tanks is an unexplored protective measure for NAPL spill containment.

Multiphase flow simulators are commonly employed to predict the spatial and temporal distributions of organic liquids at hazardous waste sites. Early modeling studies were restricted to homogeneous systems. More recently, studies have explored the role of physical heterogeneities on NAPL migration and entrapment.^{20,33,44-46} Simulations presented by Kueper and Frind⁴⁵ and Essaid and Hess³³ demonstrate that even relatively minor degrees of physical heterogeneity, can significantly affect the degree of lateral organic spreading. The correlation of intrinsic permeability and capillary pressure relations was also shown to affect the degree of lateral spreading. Kueper and Gerhard⁴⁶ investigated the influence of source size and strength on the infiltration rate and structure of a NAPL spill. Infiltration rates were found to strongly depend on the source size and permeability field correlation structure. Dekker and Abriola²⁰ observed increased sensitivity to the permeability distribution statistics and the capillary pressure-intrinsic

permeability correlation for increasing formation heterogeneity. These authors also demonstrated that the spill release rate, natural hydraulic gradient, and cross-correlation of residual saturations had only minor influence on NAPL distributions in heterogeneous formations. In general, application of multiphase flow models to laboratory and field data has demonstrated that inclusion of capillary entrapment and hysteresis is essential for accurate description of observed behavior.^{32,47,60,71} Numerical studies further indicate that immiscible flow pathways are extremely sensitive to small-scale heterogeneities in permeability and capillary characteristics.^{20,45} All reviewed numerical multiphase studies, however, have assumed that the porous media were strongly water-wet. Based upon predicted sensitivity to capillary behavior, this suggests that large errors may be introduced into numerical simulations when the water-wet assumption does not hold.

In natural subsurface systems highly irregular distributions of NAPLs have been observed.^{32,60} The superposition of physical and chemical heterogeneities in such environments will determine the flow and entrapment behavior of NAPLs. At present, very little research has investigated the influence of wettability on multiphase flow and entrapment. An improved understanding of NAPL migration and entrapment in physically and chemically heterogeneous systems should aid in the characterization of contaminant sources in the field and facilitate the development and assessment of remediation strategies. This work presents modifications to a multiphase flow simulator to account for subsurface chemical and physical heterogeneities. The numerical model is subsequently employed to explore the potential impact that wettability can have on the flow and entrapment of NAPLs in aquifer formations.

2 MODEL DESCRIPTION

The equations for the flow of two immiscible fluids in a porous medium may be written as (e.g. Abriola¹):

$$\frac{\partial}{\partial t}(\varepsilon \rho_i S_i) = \nabla \cdot \left[\mathbf{k} \frac{\rho_i k_{ri}}{\mu_i} (\nabla P_i - \rho_i g \nabla z) \right] + Q_i \quad (1)$$

where P_i is the pressure, S_i is the saturation, ε is the porosity of the medium, μ_i is the viscosity, \mathbf{k} is the intrinsic permeability, k_{ri} is the relative permeability, ρ_i is the density, g is the acceleration due to gravity, Q_i is a source/sink term, z is the positive downward vertical direction, ∇ is the two-dimensional (cross-sectional) gradient operator, and the subscript i denotes the fluid phases (i.e., $i = o, w$ for organic and water, respectively). The set of partial differential equations given by eqn (1) are coupled through the hydraulic property relations which are discussed in Sections 2.1 and 2.2 of this paper. Mass conservation requires that the following constraint is met:

$$S_o + S_w = 1 \quad (2)$$

In the work presented herein, an extensively modified form

Table 1. Reference soil parameters

Parameter	Symbol	Value
Porosity (eqn 4))	ε^{ref}	0.340
Intrinsic permeability (eqn 4))	k^{ref}	$5.00 \times 10^{-12} \text{ m}^2$
Reciprocal entry pressure (eqn 5))	α_D	$2.94 \times 10^{-4} \text{ m}^2/\text{N}$
P_c - S model parameter (eqn 5))	n	4.993
P_c - S model parameter (eqn 5))	m	0.599
Drainage pore radius (eqn 8))	$R_D^{\text{ref}}(0.5)$	$3.49 \times 10^{-3} \text{ cm}$
Imbibition pore radius (eqn 8))	$R_I^{\text{ref}}(0.5)$	$4.81 \times 10^{-3} \text{ cm}$
Interfacial tension (eqn 8))	$\sigma_{\text{ow}}^{\text{ref}}$	0.026 N/m

of the VALOR model² known as M-VALOR is used to solve the set of coupled partial differential equations given by eqn (1). M-VALOR is a finite difference code which uses an iterative implicit pressure–explicit saturation (IMPES) scheme to solve the resulting set of algebraic equations. The IMPES scheme solves a set of weakly nonlinear equations in P_w using a sparse unsymmetric linear solver employing a variant of Gauss elimination.^{29,30} Following the solution of the pressure equations, the explicit solution for the saturations is obtained using the mass balance expressions. The saturations are then updated in the pressure equation and the process is repeated until convergence is achieved. The M-VALOR model has been shown to be a robust, computationally efficient code for the simulation of a wide variety of multiphase flow problems.^{20,24,63,64}

The solution of eqn (1) requires knowledge of the fluid/matrix flow properties. The generation of spatial distributions of permeability and capillary parameters is discussed below, followed by a description of the modeling of wettability effects on these parameters. Terminology employed in this work pertaining to residual, effective, and apparent saturations under various porous medium wettability conditions is defined in Appendix A. A discussion of the influence of wettability on fluid entrapment is also provided in Appendix A. For the reader's convenience, a notation section is included at the beginning of the paper.

2.1 Spatial variability of parameters

In physically heterogeneous porous media the intrinsic permeability varies spatially with changes in soil texture. The turning bands method⁶⁹ was used in this work to generate spatially correlated heterogeneous permeability distributions for model input. This method assumes a log normal distribution of the intrinsic permeability^{68,74} with a specified mean and covariance structure. The spatial correlation structure of intrinsic permeability is described using an exponentially decaying covariance function.⁶⁸

Two methods for describing formation chemical heterogeneity are considered herein: specification of the contact angle (ϕ_{sow}) or of the organic-wet solid mass fraction (F_o). The contact angle is an index of wettability that is typically measured by placing a drop of the organic liquid on a flat solid that is immersed in water. The contact angle is then defined as the angle between the solid–water and

water–organic contact lines. Contact angles measured in this manner, however, are only a crude approximation to those governing behavior in natural porous media due to spatial variability in the local solid surface wetting characteristics. Alternatively, capillary pressure data may be used to infer an effective or ‘macroscopic’ contact angle of the porous medium (cf. Eqn (15)).^{12,55} Subsequent references to ϕ_{sow} in this work refer to such a macroscopic concept of the contact angle. When $\phi_{\text{sow}} < 90^\circ$ water is classified as the wetting fluid, whereas, for $\phi_{\text{sow}} > 90^\circ$ the water is the nonwetting fluid (neutral wettability occurs for $\phi_{\text{sow}} = 90^\circ$). Values of F_o are used herein to quantify the wettability of systems in which both water- and organic-wet solids occur at the pore-scale. Under conditions of fractional wettability, macroscopic wettability behavior has been found to depend on the saturation history.¹³

At present, there is a paucity of data on subsurface variations in wetting properties. Treiber *et al.*⁷⁰ and Chilingar and Yen¹⁹ measured contact angles for various polished core samples and petroleum reservoir fluids; however, no systematic study of contact angle variations for a single reservoir or aquifer has been reported. Some information, however, is available pertaining to the spatial variability of adsorption parameters at the field scale.^{34,65} In these and related theoretical investigations, adsorption parameters have been assumed to be correlated with subsurface physical heterogeneity.^{9,10,34,40,53,76} In this work the contact angle or organic-wet fraction is similarly considered to be correlated with the intrinsic permeability. To account for the correlation between chemical (contact angle or organic-wet fraction) and physical (intrinsic permeability) heterogeneity, the following exponential relationship is employed:

$$\xi(\mathbf{x}) = \xi_{\text{avg}} \exp[\beta(\ln(k(\mathbf{x})) - \ln(k_{\text{avg}}))] \quad (3)$$

Here ξ denotes the porous medium wettability parameter (ϕ_{sow} or F_o), \mathbf{x} is the two-dimensional spatial coordinate vector, β is the correlation coefficient, and ξ_{avg} and k_{avg} are the geometric mean of the wettability parameter and intrinsic permeability, respectively. Note that $\ln(k(\mathbf{x}))$ and $\ln(\xi(\mathbf{x}))$ are positively correlated for $0 < \beta \leq 1$, and negatively correlated for $-1 \leq \beta < 0$. Values of β closer to zero indicate a weaker correlation.

In this work, the capillary pressure (P_c)–saturation relations are directly correlated with the intrinsic permeability

field according to Leverett scaling:⁵⁰

$$P_c(\bar{S}_w^{\text{app}}, \mathbf{x}) = \left(\frac{k^{\text{ref}} \varepsilon(\mathbf{x})}{k(\mathbf{x}) \varepsilon^{\text{ref}}} \right)^{0.5} P_c^{\text{ref}}(\bar{S}_w^{\text{app}}) \quad (4)$$

where $P_c = P_o - P_w$ is defined herein with respect to water as the wetting phase, \bar{S}_w^{app} is the apparent water saturation which is defined in Appendix A, and the superscript 'ref' denotes the indicated parameters for the reference soil. Researchers have found that Leverett scaling yields reasonable predictions of P_c - S relations for unconsolidated sands^{45,50} and sandstones.³¹ Table 1 provides values of the reference parameters employed herein. In this work the porosity is assumed to be constant ($\varepsilon(\mathbf{x}) = \varepsilon^{\text{ref}}$) throughout the simulation domain.

The reference P_c - S relation in eqn (4), denoted with superscript 'ref', is described with the van Genuchten⁷² P_c - S model:

$$P_c^{\text{ref}}(\bar{S}_w^{\text{app}}) = \frac{1}{\alpha_{D,I}} \left[\bar{S}_w^{\text{app}} - \frac{1}{m} - 1 \right]^{\frac{1}{n}} \quad (5)$$

where n is related to the slope at the inflection point of the P_c - S curve, $\alpha_{D,I}$ is the reciprocal of the entry pressure that depends on whether water is draining (D) or imbibing (I), and m was chosen to be equal to $1 - 2/n$ to facilitate the implementation of the relative permeability model (eqns (12) and (13)). The reference soil was chosen such that water perfectly wets the solid surface ($\phi_{\text{sow}} = 0^\circ$). Consequently, the P_c - S relations generated for other locations according to eqn (4) are also for perfectly wetted media.

2.2 Wettability effects on hysteretic hydraulic properties

The procedure for incorporating the influence of wettability on the hydraulic property relations, at a given spatial location, is discussed below. When ϕ_{sow} is independent of saturation, wettability effects on the P_c - S relations are obtained by scaling the perfectly wetted capillary pressure relation (cf. Eqn (4)) with the macroscopic contact angle at that spatial location:

$$P_c^*(\bar{S}_w^{\text{app}}) = \cos(\phi_{\text{sow}}) P_c(\bar{S}_w^{\text{app}}) \quad (6)$$

Here \bar{S}_w^{app} is the apparent wetting fluid saturation which is defined in Appendix A, and P_c^* denotes the wettability dependent capillary pressure ($P_o - P_w$). Note that P_c^* and P_c are functions of \bar{S}_w^{app} , since P_c (cf. Eqn (4)) is also written in terms of the wetting fluid saturation. Consequently, \bar{S}_w^{app} equals \bar{S}_w^{app} for $\phi_{\text{sow}} \leq 90^\circ$, while \bar{S}_w^{app} equals \bar{S}_o^{app} for $\phi_{\text{sow}} > 90^\circ$. Hysteresis in the P_c - S relations is accounted for herein by making α_I (cf. Eqn (5)) a function of the effective minimum wetting fluid saturation ($\bar{S}_{w\text{min}}^{\text{eff}}$), which determines the maximum amount of entrapped

nonwetting fluid (cf. Appendix eqn (A7)), as:

$$\alpha_I = (2 - \bar{S}_{w\text{min}}^{\text{eff}}) \alpha_D \quad (7)$$

Recall that $\bar{S}_{w\text{min}}^{\text{eff}}$ equals the effective minimum water saturation ($\bar{S}_{w\text{min}}^{\text{eff}}$) for $\phi_{\text{sow}} < 90^\circ$, and the effective minimum organic saturation ($\bar{S}_{o\text{min}}^{\text{eff}}$) for $\phi_{\text{sow}} > 90^\circ$. The value of α_D is assumed to be constant in time. Note that $\alpha_I = 2\alpha_D$ when $\bar{S}_{w\text{min}}^{\text{eff}} = 0$ as suggested by the data presented by Kool and Parker.⁴² At saturation reversal points (a change from imbibition to drainage, or drainage to imbibition) the value of α was empirically transitioned from α_I to/from α_D over a saturation range of 0.05 to insure a smooth change in capillary pressure.

For fractional wettability soil (saturation dependent wettability) the $P_c(\bar{S}_w^{\text{app}})$ relation (eqn (4)) is 'shifted':¹⁴

$$P_c^*(\bar{S}_w^{\text{app}}) = P_c(\bar{S}_w^{\text{app}}) - \frac{\sigma_{\text{ow}} R_{D,I}^{\text{ref}}(0.5)}{\sigma_{\text{ow}}^{\text{ref}} R_{D,I}(0.5)} \lambda_{D,I}^{\text{ref}}(F_o) \quad (8)$$

where $\lambda_{D,I}^{\text{ref}}$ is the shifting parameter that depends on F_o and whether water is draining or imbibing. Here σ_{ow} is the interfacial tension, and $R_{D,I}(0.5)$ is the value of the pore radius that empties during main drainage and imbibition at an apparent water saturation equal to 0.5 ($R_{D,I}(0.5) = 2\sigma_{\text{ow}}/P_c(0.5)$). Table 1 provides values for the corresponding reference soil parameters $\sigma_{\text{ow}}^{\text{ref}}$ and $R_{D,I}^{\text{ref}}(0.5)$. Note in eqn (8) that $\lambda_{D,I}^{\text{ref}}$ is scaled by the ratios $R_{D,I}^{\text{ref}}(0.5)/R_{D,I}(0.5)$ and $\sigma_{\text{ow}}/\sigma_{\text{ow}}^{\text{ref}}$ to account for differences in the pore size and interfacial tension, respectively, of the reference system and other fluid-porous medium systems. Bradford and Leij¹⁴ derived the following regression relations, which are employed herein, from fitted values of $\lambda_{D,I}^{\text{ref}}$ (units in cm of water) to fractional wettability main drainage and imbibition P_c - S data:

$$\lambda_D^{\text{ref}}(F_o) = 11.35 * F_o + 1.81 \quad (r^2 = 0.994) \quad (9)$$

$$\lambda_I^{\text{ref}}(F_o) = 16.8 * F_o + 0.72 \quad (r^2 = 0.958) \quad (10)$$

Hysteresis in the fractional wettability P_c - S curve is also modeled by making α_I a function of the effective minimum water saturation as in eqn (7). In addition, the dependence of $\lambda_{D,I}^{\text{ref}}$ on $\bar{S}_{w\text{min}}^{\text{eff}}$ must also be considered since the porous medium is initially water saturated. In this case it is assumed that $\lambda_{D,I}^{\text{ref}}$ depends on $\bar{S}_{w\text{min}}^{\text{eff}}$ as:

$$\lambda_{\text{hys}}^{\text{ref}} = (1 - \bar{S}_{w\text{min}}^{\text{eff}}) \lambda_{D,I}^{\text{ref}} \quad (11)$$

where $\lambda_{D,I}^{\text{ref}}$ is given in eqn (9) and eqn (10), and $\lambda_{\text{hys}}^{\text{ref}}$ is the shift parameter modified for hysteresis. Note that according to eqn (11) the value of $\lambda_{\text{hys}}^{\text{ref}}$ is zero at complete water saturation, and maximum at the residual water saturation ($\lambda_{\text{hys}}^{\text{ref}} = 0$ for $\bar{S}_{w\text{min}}^{\text{eff}} = 1$, and $\lambda_{\text{hys}}^{\text{ref}} = \lambda_{D,I}^{\text{ref}}$ for $\bar{S}_{w\text{min}}^{\text{eff}} = 0$).

The influence of wettability variations on the relative permeability relations are modeled with the modified Burdine¹⁶ model according to the approach presented in

Bradford *et al.*:¹¹

expressions on the right-hand side of eqn (12) and eqn

$$k_{rw}(\bar{S}_w^{\text{app}}) = (\bar{S}_w^{\text{eff}} - \bar{S}_{wt}^{\text{eff}})^2 \frac{[1 - f(\phi_{\text{sow}})] \int_0^{\bar{S}_w^{\text{app}}} R(S)^2 dS + f(\phi_{\text{sow}}) \int_{1 - \bar{S}_w^{\text{app}}}^1 R(S)^2 dS}{\int_0^1 R(S)^2 dS} \quad (12)$$

$$k_{ro}(\bar{S}_o^{\text{app}}) = (\bar{S}_o^{\text{eff}} - \bar{S}_{ot}^{\text{eff}})^2 \frac{f(\phi_{\text{sow}}) \int_0^{\bar{S}_o^{\text{app}}} R(S)^2 dS + [1 - f(\phi_{\text{sow}})] \int_{1 - \bar{S}_o^{\text{app}}}^1 R(S)^2 dS}{\int_0^1 R(S)^2 dS} \quad (13)$$

Here \bar{S}_w^{eff} , \bar{S}_o^{eff} , $\bar{S}_{wt}^{\text{eff}}$, and $\bar{S}_{ot}^{\text{eff}}$ are the effective water, organic, entrapped water, and entrapped organic saturations, respectively, which are discussed in more detail in Appendix A, $R(S)$ is the pore radius distribution ($R(S_w) = P_c(S_w)/2\sigma_{ow}$), and S is a dummy saturation variable of integration. The empirical weighting function in eqn (12) and eqn (13), $f(\phi_{\text{sow}})$, is defined as:

$$f(\phi_{\text{sow}}) = \frac{1}{2}[1 - \cos(\phi_{\text{sow}})] \quad (14)$$

Eqn (12) and eqn (13) are based upon the division of pores into two wettability classes. The first and second

(13) are determined by the pore class of the wetting and nonwetting fluid, respectively. The wettability of the porous medium is used to determine the contributions of the pore classes to k_r according to eqn (14). Tortuosity of the flow path is empirically accounted for in eqn (12) and eqn (13) with $(\bar{S}_w^{\text{eff}} - \bar{S}_{wt}^{\text{eff}})^2$ and $(\bar{S}_o^{\text{eff}} - \bar{S}_{ot}^{\text{eff}})^2$, respectively. Eqn (12) and eqn (13) predict that an increase in the contact angle (measured through water) will be accompanied by an increase in the water k_r and a decrease in the organic k_r . Such behavior is consistent with experimental observations of Donaldson and Dean,²⁶ Owens and Archer⁵⁸ and McCaffery and Bennion.⁵²

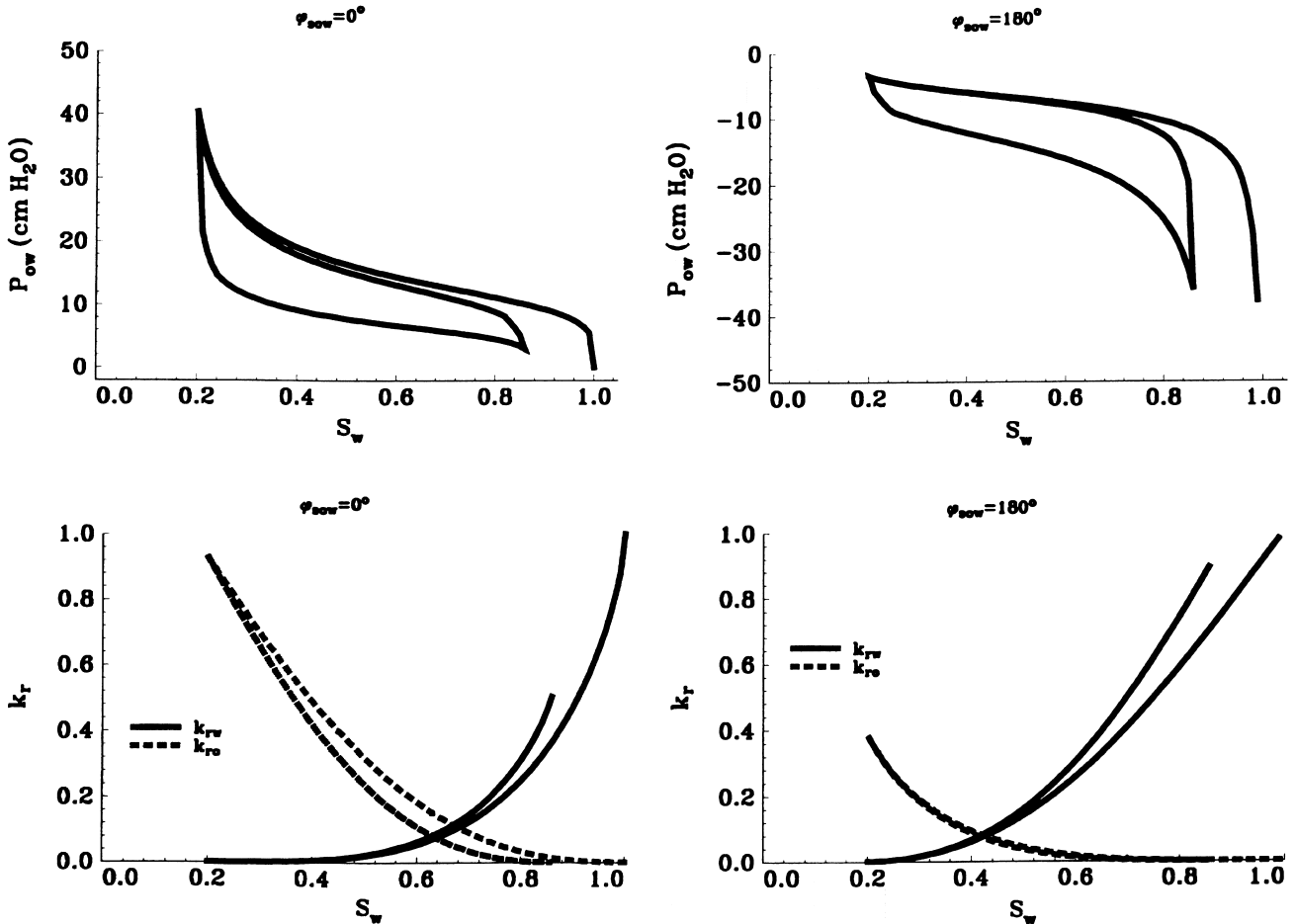


Fig. 1. Hysteretic P_c - S - k_r relations when $\phi_{\text{sow}} = 0$ and 180° .

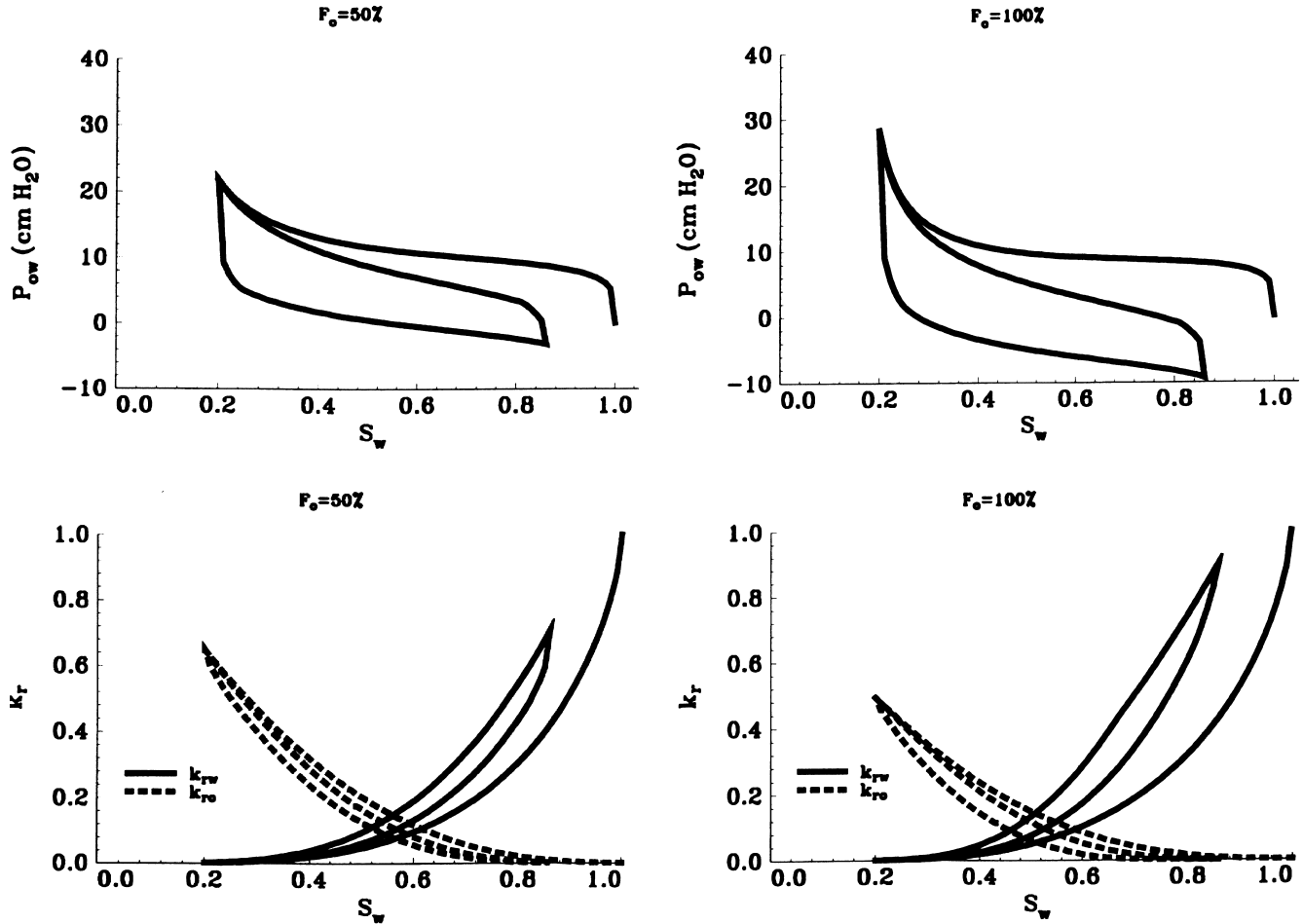


Fig. 2. Hysteretic P_c - S - k_r relations when $F_o = 50$ and 100%.

The above relative permeability relationships also depend on saturation history as a result of nonwetting fluid entrapment. Similar to the procedure of Lenhard and Parker,⁴⁹ eqn (12) and eqn (13) account for nonwetting fluid entrapment through the dependence of the relative permeabilities on apparent saturations. Additionally, the reduction in pore space accessible for fluid flow due to nonwetting fluid entrapment must be considered. This is accomplished analogous to the procedure employed by Lenhard and Parker.⁴⁹ The details of this additional modification are not given in eqn (12) and eqn (13) for simplicity.

The calculation of relative permeability relations according to eqn (12) and eqn (13) is straightforward when wettability effects are independent of saturation, i.e. when there is a constant contact angle at a given location. For the case of fractional wettability the contact angle at a given location is saturation dependent. This saturation dependence can be estimated from P_c - S data according to scaling arguments as:¹²

$$\phi_{\text{sow}}(\bar{S}_w^{\text{app}}) = \cos^{-1} \left(\frac{P_c^*(\bar{S}_w^{\text{app}})}{P_c(\bar{S}_w^{\text{app}})} \right) \quad (15)$$

where $P_c^*(\bar{S}_w^{\text{app}})$ is given by eqn (8) and $P_c(\bar{S}_w^{\text{app}})$ is given by

eqn (4). The calculated value of $\phi_{\text{sow}}(\bar{S}_w^{\text{app}})$ is subsequently used in eqns (12)–(14) to estimate the relative permeability relations.

Eqns (3)–(15) comprise the hydraulic property model that was implemented in M-VALOR to account for physical and chemical heterogeneity. To illustrate results from this constitutive model, Figs 1 and 2 show predicted hysteretic P_c - S - k_r relations when $\phi_{\text{sow}} = 0$ and 180 degrees, and when $F_o = 50$ and 100%, respectively (cf. Table 1 for reference soil characteristics). Note in Figs 1 and 2 that very different hydraulic property relations can be obtained for a given porous medium simply by assuming different wettability characteristics. The capillary pressure curves can have exclusively positive or negative values of capillary pressure ($P_{ow} = P_o - P_w$) as shown in Fig. 1, or can exhibit saturation dependent wettability effects as demonstrated in Fig. 2. Porous media with saturation dependent wettability have distinct differences in hydraulic property relations for the various drainage and imbibition cycles; i.e., positive and negative P_c which depends on the saturation history. The relative permeability relations are also dramatically influenced by wettability effects due to differences in the pore-scale fluid configuration and entrapment.

Table 2. Permeability distribution characteristics

	Case 1	Case 2	Case 3	Case 4
Mean $\ln(k)$	- 25.28	- 25.23	- 25.23	- 25.19
Variance $\ln(k)$	0.000	0.229	0.956	1.912
Horizontal correlation length (m)	∞	5.100	5.100	5.100
Vertical correlation length (m)	∞	0.210	0.210	0.210
Anisotropy factor	1.000	0.500	0.500	0.500

3 SIMULATIONS

The simulated release and redistribution of tetrachloroethylene (PCE) in one- and two-dimensional subsurface systems is presented below. The relevant physical properties of PCE that were employed in simulations are: density equal to 1625.0 kg/m^3 , viscosity equal to 0.00089 kg/ms , and interfacial tension equal to 0.045 N/m . Table 2 contains a summary of the simulated permeability distribution characteristics. Other parameters employed in the simulations are given in Table 1. Case #1 is for a physically homogeneous soil column, case #2 employs formation statistics of the Borden aquifer,⁷⁴ case #3 utilizes formation statistics similar to an aquifer characterized by Jussel *et al.*,³⁹ and case #4 is for a highly variable hypothetical aquifer. Dekker and Abriola²⁰ recently conducted a systematic investigation of the effects of physical heterogeneity on PCE infiltration and redistribution for cases #2 and #3. The influence of porous medium wettability on PCE migration and entrapment is investigated in the physically homogeneous soil column simulations (Case #1). The coupling of physical and chemical heterogeneity is explored with cases #2–#4. Note in Table 2 that physical heterogeneity increases with the variance of the natural logarithm of the intrinsic permeability. Specific information on the nodal spacing, and boundary and initial conditions is given below.

3.1 Physically homogeneous soil column

In this section results from one-dimensional simulations of PCE infiltration and redistribution into a physically homogeneous soil column (cf. Table 2 case #1) having various chemical characteristics will be presented. The model

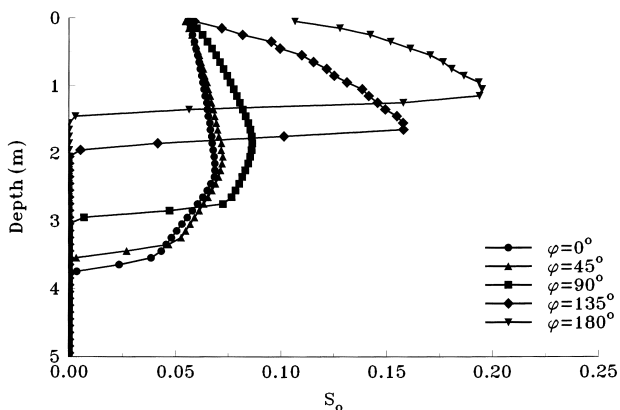


Fig. 3. PCE saturation distribution with depth after 10 days for contact angles equal to 0° , 45° , 90° , 135° , and 180° .

domain consists of an initially water saturated domain that extends 5 m in the vertical direction. Nodal spacing in the vertical direction was 0.1 m. A no flow boundary condition for water was enforced at the top of the model domain, while constant hydrostatic pressure boundary conditions (referenced to atmospheric pressure at the domain surface) were employed at the bottom boundary. A constant infiltration velocity of 1.5 cm/day of PCE was initially introduced at the top node over a period of 5 days, after which a no flow boundary condition was set at the top node while PCE was allowed to redistribute.

Fig. 3 shows the predicted PCE saturation distribution with depth (cf. Table 2 case #1) after 10 days for contact angles equal to 0° , 45° , 90° , 135° , and 180° . Demond²² reported that the contact angle for PCE measured through water was 30° on calcite, 66° on glass, and 127° on Teflon. Note in Fig. 3 that a lower depth of PCE infiltration and, hence, higher organic saturation are predicted as ϕ_{sow} increases. The observed trends in Fig. 3 occur due to decreasing k_{ro} and P_c with increasing contact angles. Hence, the mobility of the organic decreases and the porous medium retains the organic more effectively.

Fig. 4 shows the PCE saturation distribution with depth after 10 days (cf. Table 2 case #1) for porous media having organic-wet mass fractions equal to 0, 25, 50, 75, and 100%. Similar to Fig. 3, observe in Fig. 4 that a lower depth of PCE infiltration and higher organic saturation are also achieved as the organic-wet fraction increases. Comparison of Figs 3 and 4 reveals that wettability effects on the predicted saturation distribution were much more pronounced for systems having a constant contact angle (Fig. 3) than for fractional wettability media (Fig. 4). To explain these trends the dependence of $\lambda_{\text{hys}}^{\text{ref}}$ on $\bar{S}_{\text{wmin}}^{\text{eff}}$ (cf. Eqn (11)) must be

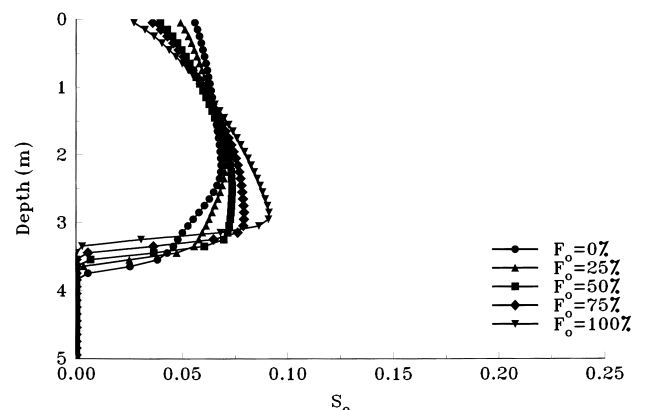


Fig. 4. PCE saturation distribution with depth after 10 days for organic-wet fractions equal to 0, 25, 50, 75, and 100%.

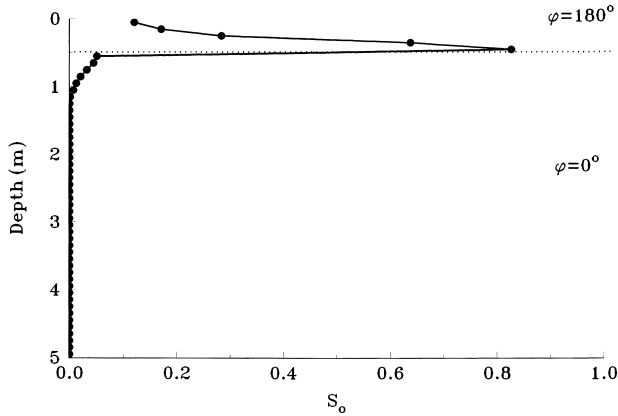


Fig. 5. PCE saturation distribution with depth after 10 days when the top 0.5 m of soil is organic-wet and the bottom 4.5 m are water-wet.

considered. For the systems shown in Fig. 4 the value of \bar{S}_{wmin}^{eff} was greater than 90% and, hence, only a small portion of the potentially organic-wet sites were exposed to organic liquid. Increasing the infiltration rate would lead to lower values of \bar{S}_{wmin}^{eff} and, consequently, the predicted organic liquid distribution would become more similar to that shown in Fig. 3.

Capillary barrier effects on organic liquid migration are known to occur at soil textural interfaces, due to abrupt changes in the pore size distribution (i.e., Wilson *et al.*⁷⁵). Barrier effects can also occur at interfaces denoting a change in soil surface wetting characteristics. Fig. 5 shows the distribution of PCE with depth after 10 days (cf. Table 2 case #1) when the top 0.5 m of soil is organic-wet and the bottom 4.5 m are water-wet. Note that very high organic saturations are achieved at the interface separating organic- and water-wet soils. Before PCE can displace water from the water-wet layer, the PCE entry pressure in this layer must be exceeded. This can only occur after the capillary pressure in the organic-wet layer approaches zero (high PCE saturations). A maximum organic saturation of 85%

Case 2 – Permeability (M^2)

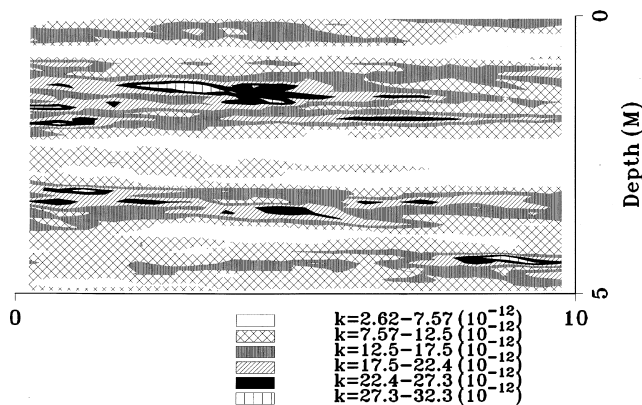


Fig. 6. Permeability distribution employed for case #2 simulations.

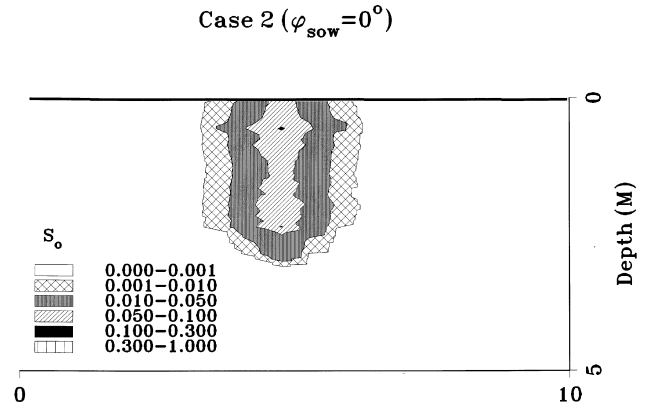
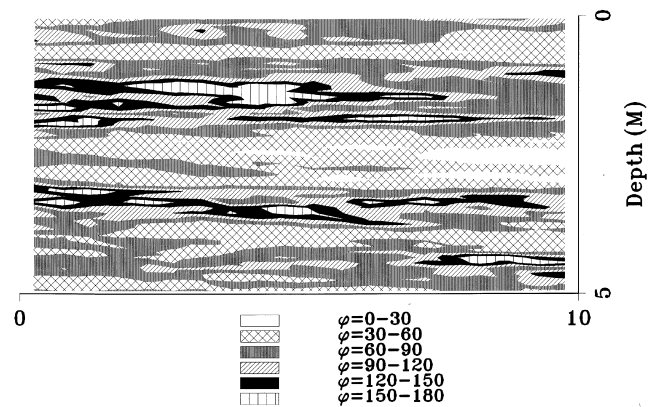


Fig. 7. PCE saturation distribution after 10 days for case #2 when $\phi_{sow} = 0^\circ$.

occurred in Fig. 5 compared with 25% in the chemically homogeneous systems (cf., Fig. 3). Fig. 5 demonstrates that organic-wet zones can create regions of high organic liquid saturation in physically homogeneous subsurface systems. This result is consistent with field observations, Atwater⁸

a) Contact Angle Case 2 ($\beta=1$)



b) Contact Angle Case 2 ($\beta=-0.5$)

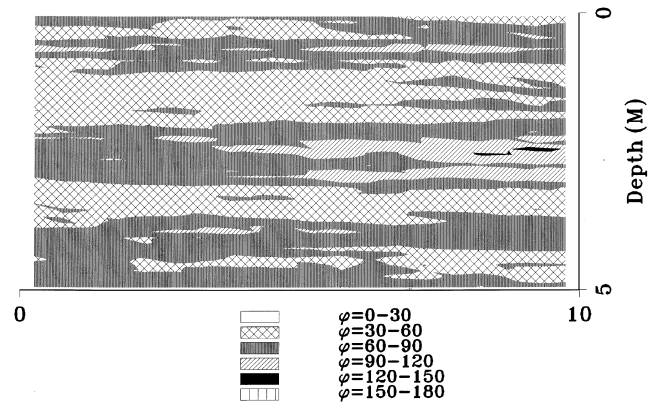


Fig. 8. Spatial distribution of ϕ_{sow} according to eqn (3) for case #2 when β is equal to 1 (a) and -0.5 (b) and the geometric mean of ϕ_{sow} is equal to 66° .

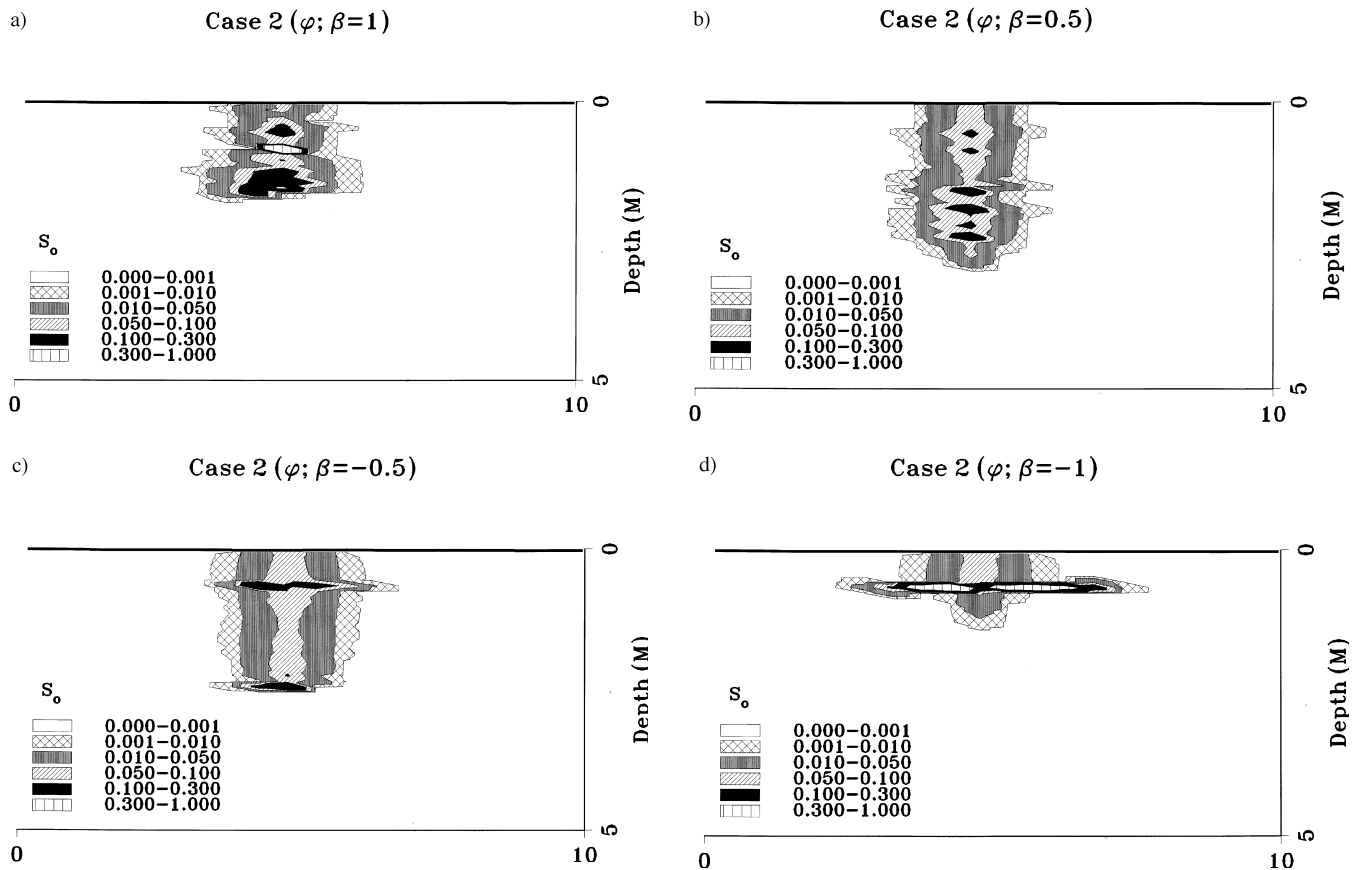


Fig. 9. Spatial distribution of PCE saturation after 10 days for case #2 when the contact angle distribution was determined according to eqn (3) with $\beta = 1.0$ (a), 0.5 (b), -0.5 (c), and -1.0 (d), and the geometric mean of ϕ_{sow} is equal to 66° .

reported the presence of high DNAPL (a dielectric fluid containing PCBs and TCB) saturations in an organic-wet clay immediately above a water-wet silt at a hazardous waste site in Regina, Canada.

3.2 Physically heterogeneous aquifers

This section presents results from two-dimensional simulations of PCE infiltration and redistribution for cases #2, #3, and #4 (cf. Table 2) having various chemical characteristics. The model domain consists of a $5 \text{ m} \times 10 \text{ m}$ vertical cross-section of an initially water saturated aquifer. Nodal spacing in the vertical and horizontal directions was 0.1 m and 0.5 m , respectively. No flow boundary conditions were enforced at the top and bottom of the model domain, while hydrostatic pressure boundary conditions were employed at the left and right boundaries (referenced to atmospheric pressure at the domain surface). A constant infiltration velocity of 3 cm/day of PCE was introduced at the top center node for a period of 5 days, after which a no flow boundary condition was maintained at this node while PCE was allowed to redistribute.

Fig. 6 shows the generated permeability distribution for case #2. The mean intrinsic permeability, and correlation lengths in the horizontal and vertical directions for this aquifer are given in Table 2. Fig. 7 shows the simulated

distribution of organic liquid saturation after 10 days for case #2 when a constant value of ϕ_{sow} equal to 0° is assumed. Note that the PCE saturation is rather symmetrically distributed below the injection point. Increased lateral spreading occurs at textural interfaces due to capillary barrier effects, even for the relatively low degrees of physical heterogeneity present in this scenario.

Simulations were subsequently conducted to examine the effects of coupled physical and chemical heterogeneity on the infiltration and redistribution of the PCE for case #2. Spatial distributions of ϕ_{sow} were first generated from the intrinsic permeability distribution according to eqn (3) with β equal to 1.0 , 0.5 , -0.5 , and -1.0 . As an illustration, Fig. 8a,b shows the spatial distribution of ϕ_{sow} with β equal to 1.0 , and -0.5 , respectively. In all cases, the mean value of ϕ_{sow} was set equal to 66° ; the reported value of the PCE contact angle measured through water on glass.²² Note that locations of higher contact angles are correlated with the coarser textured soils when $\beta > 0$, and with finer soils for $\beta < 0$. Values of β closer to zero (0.5 and -0.5) led to decreased variability in the contact angle distribution than when $\beta = 1$ or -1 .

Fig. 9a–d presents the spatial distribution of organic liquid saturation after 10 days when the contact angle distributions were determined with $\beta = 1.0$, 0.5 , -0.5 , and -1.0 , respectively. Observe in Fig. 8a,b and Fig. 9a,c that

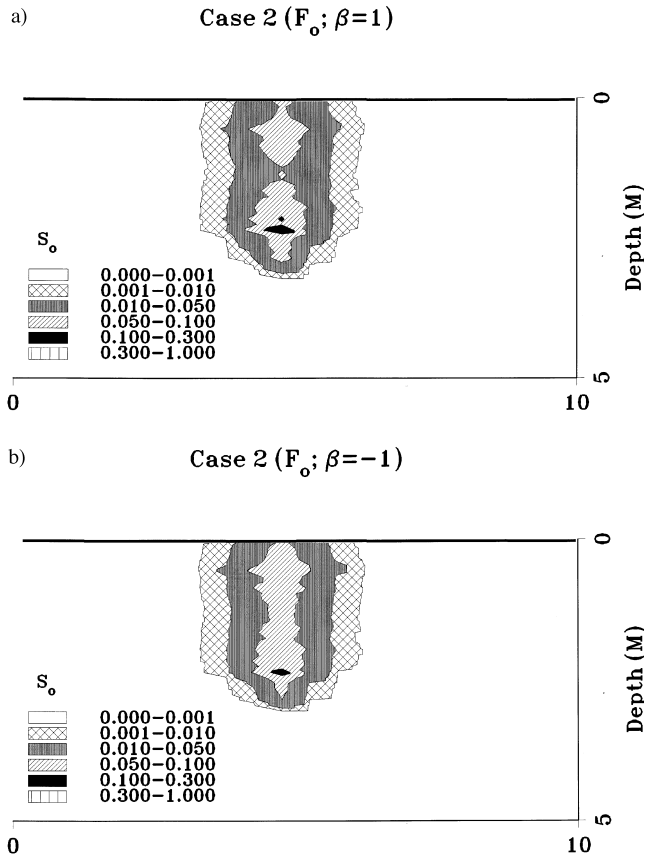


Fig. 10. Spatial distribution of PCE saturation after 10 days for case #2 when the organic-wet fraction distribution was determined according to eqn (3) with $\beta = 1$ (a) and -1 (b), and the geometric mean of F_o is equal to 36.6%.

higher organic liquid saturations occur in regions having higher contact angles. Note that the depth of PCE infiltration increases and lateral spreading decreases when $\beta = 1$ in comparison with the case $\beta = -1$ (Fig. 9a,d). Recall that, for a given contact angle, stronger capillary forces and lower intrinsic permeability occur in finer than in coarser textured soils, which will cause the organic liquid to be more forcefully retained. In Fig. 9a,d the organic liquid is primarily retained/found in the coarser and finer textured soils, respectively, due to the spatial distribution of contact angles and, consequently, the mobility of the organic is greater in Fig. 9a ($\beta = 1$) than in Fig. 9d ($\beta = -1$). Comparison of Fig. 9b ($\beta = 0.5$) and Fig. 9c ($\beta = -0.5$) reveal similar trends. In this case, however, the decreased variability in the contact angle distribution (cf. Fig. 8a,b) diminishes the potential capillary barrier effects that can occur at soil chemical property interfaces.

Comparison of Figs 7, and 9a–d demonstrate the potential importance of chemical heterogeneity on the migration of organic liquids in the subsurface. In chemically heterogeneous systems much higher organic saturations are achieved, lateral spreading is increased, and the depth of organic liquid penetration is decreased compared with the water-wet case. Similar to Fig. 5, this result can be explained by capillary barrier effects; i.e., the PCE entry

pressure of the more water-wet layer is not exceeded until the PCE saturation in the more organic-wet layer increases. Sharp contrasts in soil texture can yield similar capillary barrier effects on organic liquid migration (e.g., Kueper *et al.*⁴³).

Spatial distributions of F_o were also generated from the intrinsic permeability shown in Fig. 6 according to eqn (3) with β equal to 1 and -1 . In this case, the mean value of F_o was chosen to be equal to 36.6%, based upon the previously employed mean value of $\phi_{\text{soil}} = 66^\circ$ and the maximum contact angle of 180° ; i.e., $66/180 = 0.366$. Fig. 10a,b shows the spatial distribution of organic liquid saturation after 10 days when $\beta = 1$ and -1 , respectively. Observe that when $\beta = -1$ (Fig. 10b) the saturation distribution is almost identical to the strongly water-wet case (Fig. 7). For $\beta = 1$ (Fig. 10a) wettability effects are more pronounced than when $\beta = -1$, but still much less significant than those shown in Fig. 9d, where contact angles were independent of saturation. Similar to Fig. 4, the observed PCE saturation distribution can be explained by considering the dependence of the hydraulic properties on $\bar{S}_{\text{wmin}}^{\text{eff}}$. For a given F_o , water is retained more strongly by the finer soils than the coarser soils. Consequently, lower values of $\bar{S}_{\text{wmin}}^{\text{eff}}$ (higher organic saturation) are possible in the coarser textured soils. Hence, fractional wettability effects on the organic saturation distribution are more apparent when F_o is positively correlated with intrinsic permeability (the coarser textured media). In contrast to Fig. 10a,b, when wettability is independent of $\bar{S}_{\text{wmin}}^{\text{eff}}$ (constant contact angle) the influence on the spatial distribution of organic liquid (Fig. 9a,d) was more pronounced when $\beta = -1$ than for $\beta = 1$.

Fig. 11a,b shows the organic liquid distribution after 10 days for cases #3 and #4, respectively, when $\phi_{\text{soil}} = 0^\circ$. Comparison of Figs 7, and 11a,b reveals that increasing the variance in $\ln(k)$ leads to increased lateral spreading, and a decrease in the depth of penetration of PCE as has been previously reported.^{20,33,45} Note that higher organic saturations occur in regions of higher intrinsic permeability since finer textured soils act as a capillary barrier to organic liquid entry.

Coupled chemical and physical heterogeneity scenarios similar to those performed for case #2 were carried out for cases #3 and #4. Fig. 12a,b shows the organic liquid distribution after 10 days for cases #3 and #4, respectively, when the contact angle is perfectly correlated with the intrinsic permeability ($\beta = 1$) and the mean value of ϕ_{soil} was again set equal to 66° . Note that as the variance of the permeability increases (cf. Fig. 11a and Fig. 12a, and Fig. 11b and Fig. 12b), the influence of wettability on the organic saturation distribution becomes less apparent. Similar results were obtained when the contact angle was negatively correlated with the intrinsic permeability. This observation suggests that spatial variations in contact angles can potentially be a controlling factor of organic liquid distribution in systems with lower degrees of physical heterogeneity such as many sandy aquifer formations.^{37,39,67,68,74}

Fig. 13 shows the organic saturation distribution after 10 days for case #3 when the organic-wet fraction is perfectly

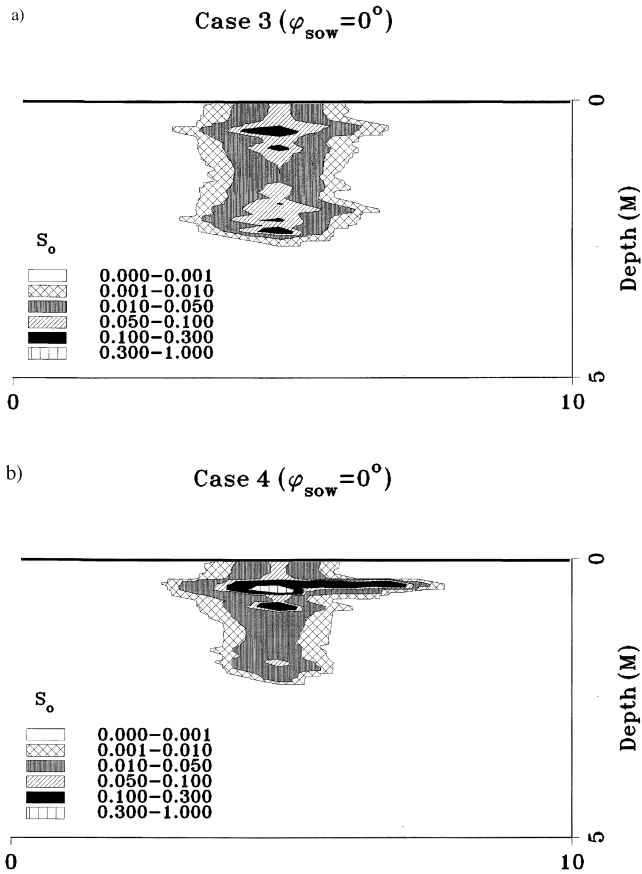


Fig. 11. Spatial distribution of PCE saturation after 10 days for cases #3 (a) and #4 (b), when $\phi_{sow} = 0^\circ$.

correlated with the intrinsic permeability ($\beta = 1$) and the mean value of F_o is again set equal to 36.6%. Comparison of the organic saturation distributions for completely water-wet and fractional wettability ($\beta = 1$) aquifers for cases #2 (Figs 7, and 10a) and #3 (Fig. 11a and Fig. 13) reveals an increased impact of fractional wettability on the distributions with increasing physical heterogeneity. This result occurs due to the dependence of the fractional wettability hydraulic property relations on the historic minimum water saturation. Increases in the permeability variance leads to sharper contrasts in soil texture (capillary barriers) which result in higher organic saturations (cf. Fig. 7, Fig. 11a, and Fig. 11b). The presence of fractional wettability further accentuates such capillary barrier effects due to its impact on the hydraulic property relations (i.e., decreasing k_{ro} and P_c at a given saturation) as S_{wmin}^{eff} decreases. In contrast, when $\ln(F_o)$ and $\ln(k)$ are inversely related ($\beta = -1$) increasing the physical heterogeneity will not greatly affect S_{wmin}^{eff} in the finer textured soils and, hence, fractional wettability has little impact on the predicted organic saturation distributions.

4 SUMMARY AND CONCLUSIONS

This work represents the first attempt to simulate the influence of wettability on organic liquid migration and

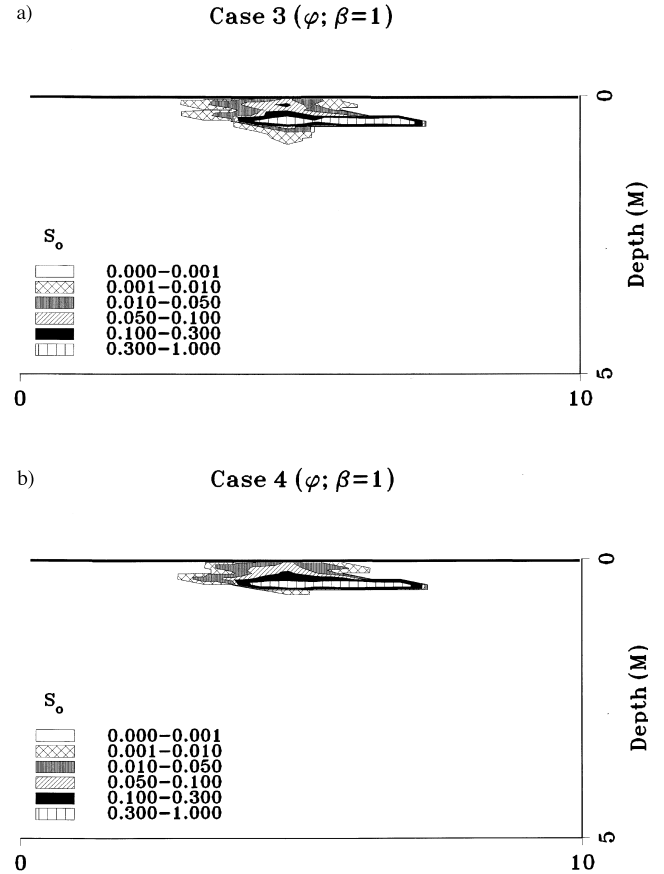


Fig. 12. Spatial distribution of PCE saturation after 10 days for cases #3 (a) and #4 (b), respectively, when the contact angle distribution was determined according to eqn (3) with $\beta = 1$ and the geometric mean of $\phi_{sow} = 66^\circ$.

entrapment. Modifications to a multiphase flow simulator are given to account for chemical, as well as, physical heterogeneities. Physical heterogeneity was simulated with a spatially variable distribution of intrinsic permeability having specified statistics and correlation structure according to the turning bands method. Soil chemical heterogeneity was assumed to alter the wettability properties of the

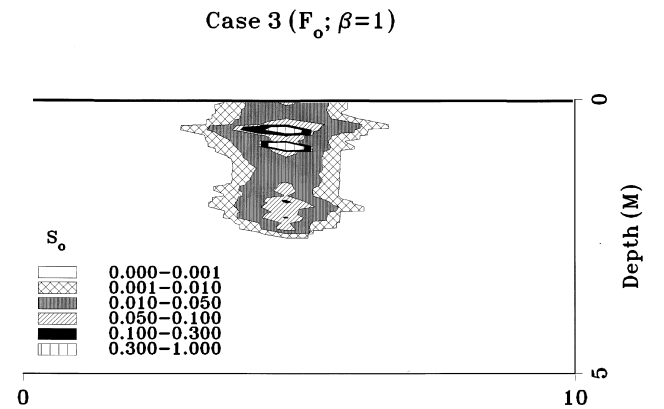


Fig. 13. Spatial distribution of PCE saturation after 10 days for case #3 when the organic-wet fraction distribution was determined according to eqn 3) with $\beta = 1$ and the geometric mean of $F_o = 36.6\%$.

subsurface through variations in contact angle or organic-wet mass fraction. Spatial distributions of chemical heterogeneity were generated by correlation with the intrinsic permeability. Capillary properties were obtained from the intrinsic permeability according to Leverett scaling. Wettability effects on the capillary pressure-saturation relations were modeled by contact angle scaling or curve 'shifting' (fractional wettability systems), according to a previously developed correlation. Wettability effects on relative permeability relations were modeled with a Burdine model, modified to weight contributions of wetting and nonwetting fluid pore classes.¹¹

One-dimensional simulations in physically homogeneous porous media demonstrated that as the contact angle or organic-wet fraction increased, the maximum organic liquid saturation increased and the depth of infiltration decreased. Wettability effects on the predicted organic saturation distribution were found to be more pronounced for increasing contact angles than for increasing organic-wet fractions (fractional wettability). This result was attributed to the dependence of the fractional wettability hydraulic properties on the historic minimum water saturation. Simulations also demonstrated that capillary barrier effects can occur at soil chemical property interfaces. The presence of such barriers can lead to dramatically higher organic liquid saturations.

Two-dimensional simulations for coupled physically and chemically heterogeneous aquifers revealed that the presence of chemical heterogeneities can dramatically influence the predicted distribution of organic saturation in aquifer formations. Higher organic saturations, increased lateral spreading, and decreased infiltration depth of the organic plume were predicted when the contact angle was negatively correlated with the intrinsic permeability. Similar effects were observed when the contact angle was positively correlated with the intrinsic permeability, but to a lesser extent due to decreased capillary forces and increased permeability of coarser textured soils. Spatial distributions of contact angles had a greater influence on the predicted organic saturation distribution for systems having a lower variance in permeability, i.e., lower degrees of physical heterogeneity. When chemical heterogeneity was represented with spatial distributions of organic-wet solid fractions, the predicted organic saturation distributions were much more similar to those for the perfectly water-wet scenarios. In general, fractional wettability effects on organic saturation distributions were found to be more pronounced for systems which achieved lower water saturations; i.e., when the organic-wet fraction was positively correlated with the intrinsic permeability, and for systems having a larger variance in permeability. As in the one-dimensional case, these observations were attributed to the dependence of the fractional wettability hydraulic properties on the historic minimum water saturation.

There is presently a need to quantify the spatial distribution of wettability properties in natural aquifer formations. Results presented herein indicate that knowledge of the wettability distribution may be of at least equal importance

as the intrinsic permeability distribution in some systems. The evolution of wettability as a function of saturation and concentration history is another area which should be addressed in future studies. Work is ongoing to test and refine the modeling of wettability effects on hydraulic property relations. A more complete understanding of the influence of wettability on entrapment and capillary behavior may also lead to improved methods for aquifer remediation and control of organic liquid migration.

ACKNOWLEDGEMENTS

Funding for this research was provided by the Department of Energy under Grant # DE-FG07-96ER14702. The research described in this article has not been subject to Agency review and no official endorsement should be inferred.

REFERENCES

1. Abriola, L. M. Modeling multiphase migration of organic chemicals in groundwater systems—A review and assessment. *Environ. Health Perspect.*, 1989, **83**, 117–143.
2. Abriola, L. M., Rathfelder, K., Maiza, M. and Yadav, S., VALOR code version 1.0: A PC code for simulating immiscible contaminant transport in subsurface systems, EPRI TR-101018, Project 2879-08, Final Report, September, 1992.
3. Al-Fossail, K. and Handy, L. L. Correlation between capillary number and residual saturation. *J. Colloid Interface Sci.*, 1990, **134**, 256–263.
4. Anderson, W. G. Wettability literature survey—Part 1: Rock/oil/brine interactions and the effects of core handling on wettability. *J. Petrol. Technol.*, 1986, **38**, 1125–1144.
5. Anderson, W. G. Wettability literature survey—Part 2: Wettability measurement. *J. Petrol. Technol.*, 1986, **38**, 1246–1261.
6. Anderson, W. G. Wettability literature survey—Part 4: Effects of wettability on capillary pressure. *J. Petrol. Technol.*, 1987, **39**, 1283–1300.
7. Anderson, W. G. Wettability literature survey—Part 5: The effects of wettability on relative permeability. *J. Petrol. Technol.*, 1987, **39**, 1453–1467.
8. Atwater, J. W. A case study of a chemical spill: Polychlorinated biphenyls (PCBs) revisited. *Water Resour. Res.*, 1984, **20**, 317–319.
9. Bellin, A., Rinaldo, A., Bosma, W. J. P., van der Zee, S. E. A. T. M. and Rubin, Y. Linear equilibrium adsorbing solute transport in physically and chemically heterogeneous porous formations, 1. Analytical solutions. *Water Resour. Res.*, 1993, **29**, 4019–4031.
10. Bosma, W. J. P., Bellin, A., van der Zee, S. E. A. T. M. and Rinaldo, A. Linear equilibrium adsorbing solute transport in physically and chemically heterogeneous porous formations, 2. Numerical results. *Water Resour. Res.*, 1993, **29**, 4031–4043.
11. Bradford, S. A., Abriola, L. M. and Leij, F. J. Wettability effects on two- and three-fluid relative permeabilities. *J. Contam. Hydrol.*, 1997, **28**, 171–191.
12. Bradford, S. A. and Leij, F. J. Wettability effects on scaling two- and three-fluid capillary pressure-saturation relations. *Environ. Sci. Technol.*, 1995, **29**, 1446–1455.

13. Bradford, S. A. and Leij, F. J. Fractional wettability effects on two- and three-fluid capillary pressure–saturation relationships. *J. Contam. Hydrol.*, 1995, **20**, 89–109.
14. Bradford, S. A. and Leij, F. J. Predicting two- and three-fluid capillary pressure–saturation relationships in fractional wettability media. *Water Resour. Res.*, 1996, **32**, 251–260.
15. Brown, R. J. S. and Fatt, I. Measurements of fractional wettability of oilfield rocks by the nuclear magnetic relaxation method. *Trans. Am. Inst. Min. Metall. Pet. Eng.*, 1956, **207**, 262–264.
16. Burdine, N. T. Relative permeability calculations from pore-size distribution data. *Trans. Am. Inst. Min. Metall. Pet. Eng.*, 1953, **198**, 71–77.
17. Burris, D. R. and Antworth, C. P. *In situ* modification of an aquifer material by a cationic surfactant to enhance retardation of organic contaminants. *J. Contam. Hydrol.*, 1992, **10**, 325–337.
18. Chatzis, I., Morrow, N. R. and Lim, H. T. Magnitude and detailed structure of residual oil saturation. *Soc. Petrol. Eng. J.*, 1983, **23**, 311–326.
19. Chilingar, G. V. and Yen, T. F. Some notes on wettability and relative permeabilities of carbonate reservoir rocks, II. *Energy Sources*, 1983, **7**, 67–75.
20. Dekker, T. J. and Abriola, L. M., The influence of field-scale heterogeneity on the infiltration and entrapment of dense nonaqueous phase liquids in saturated formations. *J. Contam. Hydrol.*, submitted.
21. Dekker, L. W. and Ritsema, C. J. How water moves in a water repellent sandy soil, I, potential and actual water repellency. *Water Resour. Res.*, 1994, **30**, 2507–2519.
22. Demond, A. H., Capillarity in two-phase liquid flow of organic contaminants in groundwater. Ph.D. thesis. Stanford University, Stanford, CA, 211 pp., 1988.
23. Demond, A. H., Desai, F. N. and Hayes, K. F. Effect of cationic surfactants on organic liquid–water capillary pressure–saturation relationships. *Water Resour. Res.*, 1994, **30**, 333–342.
24. Demond, A. H., Rathfelder, K. and Abriola, L. M. Simulation of organic liquid flow in porous media using estimated and measured transport properties. *J. Contam. Hydrol.*, 1996, **22**, 223–240.
25. Demond, A. H. and Roberts, P. V. Effect of interfacial forces on two-phase capillary pressure–saturation relationships. *Water Resour. Res.*, 1991, **27**, 423–437.
26. Donaldson, E. C. and Dean, G. W., *Two- and Three-phase Relative Permeability Studies*. U.S. Bureau of Mines, Report #6826, Washington, DC, 1966.
27. Donaldson, E. C. and Thomas, R. D., Microscopic observations of oil displacement in water-wet and oil-wet systems, SPE paper # 3555, SPE Annual Meetings, New Orleans, LA, 1971.
28. Donaldson, E. C., Thomas, R. D. and Lorenz, P. B. Wettability determination and its effect on recovery efficiency. *Soc. Petrol. Eng. J.*, 1969, **9**, 13–20.
29. Duff, I. S., MA28—A set of fortran subroutines for sparse asymmetric linear equations, Report No. AERE-R.8730, AERE Harwell Laboratories, Oxford, UK, 1979.
30. Duff, I. S., Enhancements to the MA32 package for solving sparse asymmetric equations, Report No. AERE-R.11009, AERE Harwell Laboratories, Oxford, UK, 1989.
31. Dumore, J. M. and Schols, R. S. Drainage capillary-pressure functions and the influence of connate water. *Soc. Petrol. Eng. J.*, 1974, **14**, 437–444.
32. Essaid, H. I., Herkelrath, W. N. and Hess, K. M. Simulation of fluid distributions observed at a crude oil spill site incorporating hysteresis, oil entrapment, and spatial variability of hydraulic properties. *Water Resour. Res.*, 1993, **29**, 1753–1770.
33. Essaid, H. I. and Hess, K. M. Monte Carlo simulations of multiphase flow incorporating spatial variability of hydraulic properties. *Ground Water*, 1993, **31**, 123–134.
34. Garabedian, S. P., LeBlanc, D. R., Gelhar, L. W. and Celia, M. A. Large-scale natural gradient tracer test in sand and gravel, Cape Cod, Massachusetts, 2, Analysis of spatial moments for a nonreactive tracer. *Water Resour. Res.*, 1991, **27**, 911–924.
35. Hayworth, J. S. and Burris, D. R. Nonionic surfactant-enhanced solubilization and recovery of organic contaminants from within cationic surfactant-enhanced sorbent zones. 1. Experiments. *Environ. Sci. Technol.*, 1997, **31**, 1277–1283.
36. Hayworth, J. S. and Burris, D. R. Nonionic surfactant-enhanced solubilization and recovery of organic contaminants from within cationic surfactant-enhanced sorbent zones. 2. Numerical Simulations. *Environ. Sci. Technol.*, 1997, **31**, 1284–1289.
37. Hess, K. M., Wolf, S. H. and Celia, M. A. Large-scale natural gradient tracer test in sand and gravel, Cape Cod, Massachusetts. 3. Hydraulic conductivity variability and calculated macrodispersivities. *Water Resour. Res.*, 1992, **28**, 2011–2027.
38. Hoag, G. E. and Marley, M. C. Gasoline residual saturation in unsaturated uniform aquifer materials. *J. Environ. Eng.*, 1986, **112**, 586–604.
39. Jussel, P., Stauffer, F. and Dracos, T. Transport modeling in heterogeneous aquifers: 1. Statistical description and numerical generation of gravel deposits. *Water Resour. Res.*, 1994, **30**, 1803–1817.
40. Kabala, Z. J. and Sposito, G. A stochastic model of reactive solute transport with time-varying velocity in a heterogeneous aquifer. *Water Resour. Res.*, 1991, **27**, 341–350.
41. Kia, S. F. and Abdul, A. S. Retention of diesel fuel in aquifer material. *ASCE J. Hydrol. Eng.*, 1990, **116**, 881–894.
42. Kool, J. B. and Parker, J. C. Development and evaluation of closed-form expressions for hysteretic soil hydraulic properties. *Water Resour. Res.*, 1987, **23**, 105–114.
43. Kueper, B. H., Abbott, W. and Farquhar, G. Experimental observations of multiphase flow in heterogeneous porous media. *J. Contam. Hydrol.*, 1989, **5**, 83–95.
44. Kueper, B. H. and Frind, E. O. Two-phase flow in heterogeneous porous media 1. Model development. *Water Resour. Res.*, 1991, **27**, 1049–1057.
45. Kueper, B. H. and Frind, E. O. Two-phase flow in heterogeneous porous media 2. Model application. *Water Resour. Res.*, 1991, **27**, 1059–1070.
46. Kueper, B. H. and Gerhard, J. I. Variability of point source infiltration rates for two-phase flow in heterogeneous porous media. *Water Resour. Res.*, 1995, **31**, 2971–2980.
47. Kueper, B. H., Redman, D., Starr, R. C., Reitsma, S. and Mah, M. A field experiment to study the behavior of tetrachloroethylene below the water table: Spatial distribution of residual and pooled DNAPL. *Ground Water*, 1993, **31**, 756–766.
48. Land, C. S. Calculation of imbibition relative permeability for two- and three-phase flow from rock properties. *Soc. Petrol. Eng. J.*, 1968, **8**, 149–156.
49. Lenhard, R. J. and Parker, J. C. A model for hysteretic constitutive relations governing multiphase flow 2. Permeability–saturation relations. *Water Resour. Res.*, 1987, **23**, 2197–2206.
50. Leverett, M. C. Capillary behavior in porous solids. *Trans. Am. Inst. Min. Metall. Pet. Eng.*, 1941, **142**, 152–169.
51. Lorenz, P. B., Donaldson, E. C. and Thomas, R. D., Use of centrifugal measurements of wettability to predict oil recovery, Report 7873, USBM, Barlesville Energy Technology Center, 1974.

52. McCaffery, F. G. and Bennion, D. W. The effect of wettability on two-phase relative permeabilities. *J. Can. Petrol. Technol.*, 1974, **13**, 42–53.
53. Miralles-Wilhelm, F. and Gelhar, L. W. Stochastic analysis of sorption macrokinetics in heterogeneous aquifers. *Water Resour. Res.*, 1996, **32**, 1541–1549.
54. Morrow, N. R. The effects of surface roughness on contact angle with special reference to petroleum recovery. *J. Can. Petrol. Technol.*, 1975, **14**, 42–53.
55. Morrow, N. R. Capillary pressure correlations for uniformly wetted porous media. *J. Can. Petrol. Technol.*, 1976, **15**, 49–69.
56. Morrow, N. R. Wettability and its effect on oil recovery. *J. Petrol. Technol.*, 1990, **42**, 1476–1484.
57. Morrow, N. R. and Mungan, N., Wettability and Capillarity in Porous Media, Report RR-7, Petroleum Reservoir Research Inst., Calgary, Canada, January, 1971.
58. Owens, W. W. and Archer, D. L. The effect of rock wettability on oil–water relative permeability relationships. *J. Petrol. Technol.*, 1971, **23**, 873–878.
59. Parker, J. C. and Lenhard, R. J. A model for hysteretic constitutive relations governing multiphase flow. 1. Saturation–pressure relations. *Water Resour. Res.*, 1987, **23**, 2187–2196.
60. Poulsen, M. and Kueper, B. H. A field experiment to study the behavior of tetrachloroethylene in unsaturated porous media. *Environ. Sci. Technol.*, 1992, **26**, 889–895.
61. Powers, S. E., Dissolution of nonaqueous phase liquids in saturated subsurface systems. Doctoral Thesis, The University of Michigan, 1992.
62. Powers, S. E. and Tamblin, M. E. Wettability of porous media after exposure to synthetic gasolines. *J. Contam. Hydrol.*, 1995, **19**, 105–125.
63. Rathfelder, K. and Abriola, L. M. Mass conservative numerical solutions of the head-based Richards equation. *Water Resour. Res.*, 1994, **30**, 2579–2586.
64. Rathfelder, K. and Abriola, L. M., On the influence of capillarity in the modeling of organic liquid redistribution in two-phase systems. *Advances in Water Resources*, 1988, **21**, 159–170.
65. Roberts, P. V., Goltz, M. N. and Mackay, D. M. A natural gradient experiment on solute transport in a sand aquifer. 3. Retardation estimates and mass balances for organic solutes. *Water Resour. Res.*, 1986, **22**, 2047–2058.
66. Salathiel, R. A. Oil recovery by surface film drainage in mixed-wettability rocks. *J. Petrol. Technol.*, 1973, **255**, 1212–1224.
67. Smith, L. Spatial variability of flow parameters in a stratified sand. *Mathematical Geology*, 1981, **13**, 1–21.
68. Sudicky, E. A. A natural gradient experiment on solute transport in a sand aquifer: Spatial variability of hydraulic conductivity and its role in the dispersion process. *Water Resour. Res.*, 1986, **22**, 2069–2082.
69. Tompson, A. F. B., Ababou, R. and Gelhar, L. W. Implementation of the three-dimensional turning bands random field generator. *Water Resour. Res.*, 1989, **25**, 2227–2243.
70. Treiber, L. E., Archer, D. L. and Owens, W. W. Laboratory evaluation of the wettability of fifty-five oil producing reservoirs. *Soc. Petrol. Eng. J.*, 1972, **12**, 531.
71. van Geel, P. J. and Sykes, J. F. Laboratory and model simulations of a LNAPL spill in a variably-saturated sand, 2. Comparison of laboratory and model results. *J. Contam. Hydrol.*, 1994, **17**, 27–53.
72. van Genuchten, M. Th. A closed form equation for predicting the hydraulic conductivity of unsaturated soils. *Soil Sci. Soc. Am. J.*, 1980, **44**, 892–898.
73. Wilson, J. L., Conrad, S. H., Mason, W. R., Peplinski, W. and Hagan, E., Laboratory investigation of residual liquid organics from spills, leaks and the disposal of hazardous wastes in groundwater, EPA/600/6-90/004, 1990.
74. Woodbury, A. D. and Sudicky, E. A. The geostatistical characteristics of the Borden aquifer. *Water Resour. Res.*, 1991, **27**, 533–546.
75. Xu, S. and Boyd, S. A. Cationic surfactant sorption to a vermiculitic subsoil via hydrophobic bonding. *Environ. Sci. Technol.*, 1995, **29**, 312–320.
76. Yang, J., Zhang, R. and Wu, J. Stochastic analysis of adsorbing solute transport in two-dimensional unsaturated soils. *Water Resour. Res.*, 1996, **32**, 2747–2756.

APPENDIX A

It is anticipated that soil texture will have an influence on residual saturations. Following Dekker and Abriola,²⁰ to account for this effect, the following regression relationships were employed herein:

$$S_{rw} = -0.62329 - 0.06404 \log(k) \quad r^2 = 0.997 \quad (A1)$$

$$S_{ro} = -0.52465 - 0.06234 \log(k) \quad r^2 = 0.937 \quad (A2)$$

These relations were developed from consideration of published data for measured residuals in unconsolidated media.^{3,38,41,61} eqn (A1) and eqn (A1) indicate a negative correlation between residual saturation and the log of permeability. It is assumed herein that the values of S_{rw} and S_{ro} calculated from eqn (A2) and eqn (A2) correspond to the residual saturations for perfectly water-wet porous media. Wettability effects on residual saturations are discussed below.

Researchers in the petroleum industry have investigated the effects of wettability on residual saturations.^{51,55,57} Results of Morrow and Mungan⁵⁷ and Morrow⁵⁵ suggest that the residual wetting fluid saturation decreases when ϕ_{sow} increases from 0° to 90°. The dependence of residual nonwetting fluid saturation on contact angle is not as clear. Morrow⁵⁵ found that residual nonwetting fluid saturation increased when ϕ_{sow} increases from 0° to 90°, whereas results from Lorenz *et al.*⁵¹ suggest the opposite trend. It is generally accepted, however, that S_{ro} is lowest in media with neutral wettability.⁵⁶ For this work the following expressions are employed to describe wettability effects on the residual water saturation:

$$\frac{S_{rw}^*}{S_{rw}} = 1.0 - 0.6 \left(\frac{\xi}{\xi_n} \right) \quad \frac{\xi}{\xi_n} \leq 0.5 \quad (A3)$$

$$\frac{S_{rw}^*}{S_{rw}} = 1.0 - 0.6 \left(1 - \frac{\xi}{\xi_n} \right) \quad \frac{\xi}{\xi_n} > 0.5 \quad (A4)$$

where S_{rw}^* is the residual water saturation that now accounts for wettability effects, and ξ_n is a normalizing factor for the selected wettability parameter. The value of ξ_n is equal to 180° when $\xi = \phi_{sow}$, and equal to 1 when $\xi = F_o$. Note that S_{rw} is obtained from eqn (A1). Analogous expressions to that given in eqns (A3) and (A4) were employed to describe wettability effects on S_{ro} (S_{ro}^*). Eqns (A3) and (A4) are roughly based on the data presented by Morrow.⁵⁵

To account for hysteretic wettability effects on the hydraulic property relations it is necessary to distinguish between ‘immobile’ and ‘entrapped’ residual saturations. An ‘immobile’ wetting fluid residual occurs due to the presence of thin films coating solid surfaces, whereas ‘entrapped’ nonwetting fluid residual occurs in larger portions of the pore space as wetting fluid invades due to capillary instabilities. Immobile and entrapped residual saturations will be denoted below with subscripts ‘i’ and ‘t’, respectively. It is assumed herein that only water is immobile when $\phi_{\text{sow}} < 90^\circ$ and, hence, $S_{\text{wi}} = S_{\text{rw}}^*$ and $S_{\text{oi}} = 0$. For $\phi_{\text{sow}} > 90^\circ$, only the organic liquid is assumed to be immobile, but in this case S_{oi} also depends on the portion of the pore space that has been exposed to organic liquid. Hence, it is assumed that $S_{\text{oi}} = S_{\text{ro}}^* S_{\text{omax}}$ (S_{omax} is the historic maximum organic saturation), while $S_{\text{wi}} = 0$. For fractional wettability media S_{rw}^* and S_{ro}^* are the sum of residual wetting and nonwetting water and organic saturations, respectively. Hence, it is assumed that $S_{\text{wi}} = (1 - F_o) \times S_{\text{rw}}^*$ and $S_{\text{oi}} = F_o \times S_{\text{ro}}^* \times S_{\text{omax}} / (1 - S_{\text{wi}})$. A discussion of the entrapped residual saturations is given below.

Throughout this paper the hydraulic property relations were written in terms of effective and apparent saturations. Effective saturation reflects the ‘mobile’ liquid saturation, whereas apparent saturation reflects the ‘mobile + entrapped’ liquid saturation. Effective and apparent saturations are defined herein as:

$$\begin{aligned} \bar{S}_{\text{w}}^{\text{app}} &= \frac{S_{\text{w}} - S_{\text{wi}}}{1 - S_{\text{wi}} - S_{\text{oi}}} + \frac{S_{\text{ot}}}{1 - S_{\text{wi}} - S_{\text{oi}}} - \frac{S_{\text{wt}}}{1 - S_{\text{wi}} - S_{\text{oi}}} \\ &= \bar{S}_{\text{w}}^{\text{eff}} + \bar{S}_{\text{ot}}^{\text{eff}} - \bar{S}_{\text{wt}}^{\text{eff}} \end{aligned} \quad (\text{A5})$$

$$\begin{aligned} \bar{S}_{\text{o}}^{\text{app}} &= \frac{S_{\text{o}} - S_{\text{oi}}}{1 - S_{\text{wi}} - S_{\text{oi}}} + \frac{S_{\text{wt}}}{1 - S_{\text{wi}} - S_{\text{oi}}} - \frac{S_{\text{ot}}}{1 - S_{\text{wi}} - S_{\text{oi}}} \\ &= \bar{S}_{\text{o}}^{\text{eff}} + \bar{S}_{\text{wt}}^{\text{eff}} - \bar{S}_{\text{ot}}^{\text{eff}} \end{aligned} \quad (\text{A6})$$

where $\bar{S}_{\text{w}}^{\text{app}}$ and $\bar{S}_{\text{o}}^{\text{app}}$ are the apparent water and organic saturation, respectively, $\bar{S}_{\text{w}}^{\text{eff}}$ and $\bar{S}_{\text{o}}^{\text{eff}}$ are the effective

mobile water and organic saturation, respectively, $\bar{S}_{\text{wt}}^{\text{eff}}$ and $\bar{S}_{\text{ot}}^{\text{eff}}$ are the effective entrapped water and organic saturation, respectively. The determination of $\bar{S}_{\text{wt}}^{\text{eff}}$ and $\bar{S}_{\text{ot}}^{\text{eff}}$ is discussed below.

When the porous medium is water-wet ($\phi_{\text{sow}} < 90^\circ$), the maximum effective entrapped organic saturation ($\bar{S}_{\text{mot}}^{\text{eff}}$) is determined with the procedure of Land⁴⁸ as

$$\bar{S}_{\text{mot}}^{\text{eff}} = \frac{1 - \bar{S}_{\text{wmin}}^{\text{eff}}}{1 + C(1 - \bar{S}_{\text{wmin}}^{\text{eff}})} \quad (\text{A7})$$

where $\bar{S}_{\text{wmin}}^{\text{eff}}$ is the historic minimum effective water saturation and C is given as:

$$C = \frac{1 - S_{\text{wi}}}{S_{\text{ro}}^*} - 1 \quad (\text{A8})$$

The effective entrapped organic liquid saturation ($\bar{S}_{\text{ot}}^{\text{eff}}$) as a function of effective water saturation is subsequently determined by linear interpolation as:⁵⁹

$$\bar{S}_{\text{ot}}^{\text{eff}} = \bar{S}_{\text{mot}}^{\text{eff}} \left(\frac{\bar{S}_{\text{w}}^{\text{eff}} - \bar{S}_{\text{wmin}}^{\text{eff}}}{1 - \bar{S}_{\text{wmin}}^{\text{eff}} - \bar{S}_{\text{mot}}^{\text{eff}}} \right) \quad (\text{A9})$$

Note that $\bar{S}_{\text{ot}}^{\text{eff}} = 0$ when $\bar{S}_{\text{w}}^{\text{eff}} = \bar{S}_{\text{wmin}}^{\text{eff}}$ and $\bar{S}_{\text{ot}}^{\text{eff}} = \bar{S}_{\text{mot}}^{\text{eff}}$ when $\bar{S}_{\text{w}}^{\text{eff}} = 1 - \bar{S}_{\text{mot}}^{\text{eff}}$. For a porous medium that is organic-wet ($\phi_{\text{sow}} > 90^\circ$), eqn (A7), eqn (A8), and eqn (A9) can also be used to determine the effective entrapped water saturation ($\bar{S}_{\text{wt}}^{\text{eff}}$) by reversing the roles of water and the organic liquid. For a fractional wettability medium both entrapped organic and water occur due to the presence of water- and organic-wet solids, respectively. In this case, eqn (A7) and eqn (A9) are again used to determine $\bar{S}_{\text{mot}}^{\text{eff}}$ and $\bar{S}_{\text{ot}}^{\text{eff}}$, respectively, but this time S_{ro}^* in eqn (A8) is replaced by $(1 - F_o) \times S_{\text{ro}}^*$ since S_{ro}^* is now the sum of residual wetting and nonwetting organic saturation. A similar procedure is employed to obtain $\bar{S}_{\text{mwt}}^{\text{eff}}$ and $\bar{S}_{\text{wt}}^{\text{eff}}$ after writing eqns (A7), (A8) and (A9) in terms of the organic as the wetting fluid; this time S_{ro}^* and S_{iw} are replaced by $F_o \times S_{\text{rw}}^*$ and S_{io} , respectively.